Catalysis Science & Technology

Accepted Manuscript

This is an *Accepted Manuscript*, which has been through the Royal Society of Chemistry peer review process and has been accepted for publication.

Accepted Manuscripts are published online shortly after acceptance, before technical editing, formatting and proof reading. Using this free service, authors can make their results available to the community, in citable form, before we publish the edited article. We will replace this *Accepted Manuscript* with the edited and formatted *Advance Article* as soon as it is available.

You can find more information about *Accepted Manuscripts* in the Information for Authors.

Please note that technical editing may introduce minor changes to the text and/or graphics, which may alter content. The journal's standard Terms & Conditions and the Ethical guidelines still apply. In no event shall the Royal Society of Chemistry be held responsible for any errors or omissions in this *Accepted Manuscript* or any consequences arising from the use of any information it contains.

ROYAL SOCIETY OF CHEMISTRY

www.rsc.org/catalysis

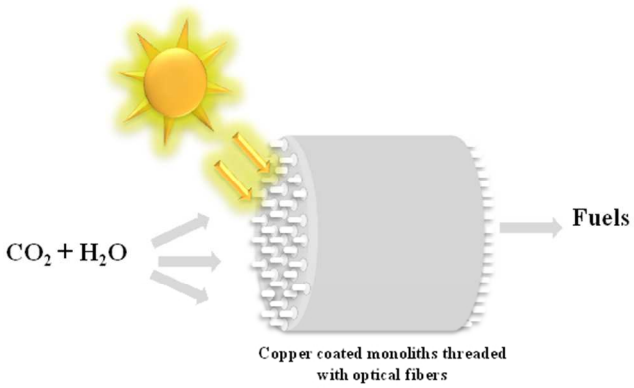

Copper based TiO2 monolithic structures threaded with optical fibers exhibit better activity than pure TiO2 for CO2 reduction under visible or UV light irradiation.
250x129mm (96 x 96 DPI)

Catalysis Science & Technology Accepted Manuscript

Cite this: DOI: 10.1039/c0xx00000x

www.rsc.org/xxxxxx

ARTICLE TYPE

Copper based TiO_2 honeycomb monoliths for CO_2 photoreduction

Oluwafunmilola Ola,*[a] and M. Mercedes Maroto-Valer[a]

Received (in XXX, XXX) Xth XXXXXXXXX 20XX, Accepted Xth XXXXXXXXX 20XX
DOI: 10.1039/b000000x

The direct photoreduction of CO_2 via catalytic conversion of copper supported on TiO_2 based monolithic structures is a means by which solar fuels can be produced. Copper based monolithic structures with varying loadings were synthesized through sol-gel dip coating procedure and tested for CO_2 reduction with H_2O as a reductant in gaseous phase. Results established that increased copper concentration can decrease crystalline size and promote anatase to rutile phase transformation. The coated monolithic structures were dominated by mainly Cu^{1+} species, as confirmed by XPS while bulk characterization suggests that these species are present in the crystal lattice via substitution of Ti^{4+} ions with Cu^{1+} ions. The catalytic performance of the Cu doped TiO_2 monoliths for hydrocarbon formation was found to be considerably higher when compared to pure TiO_2 under UVA or visible light irradiation.

1. Introduction

The utilization of carbon dioxide (CO2) for photocatalytic reduction driven by solar energy is a promising strategy for producing sustainable fuels that are suitable for use in existing energy infrastructure. Although the feasibility of using titanium dioxide (TiO2) based materials for UV induced photocatalysis have been demonstrated 1-2, its visible light applications are limited.3 The tailoring of the properties of titanium dioxide (TiO2) by the addition of metals that are relatively inexpensive and readily available for CO2 photoreduction systems is highly desirable. In this regard, the use of copper species has been increasingly investigated.4

Several researchers have reported that Cu2+ species were the active sites on Cu based TiO2 catalysts for the degradation of rhodamine B 5, photocatalytic water splitting 6 and CO2 reduction.7-8 For CO2 reduction studies, it is generally accepted that CuO can trap photoexcited electrons from the conduction band of TiO2 and these trapped elections can participate in reduction reactions with the surface adsorbed species thus preventing electron-hole recombination.1 Furthermore, previous studies have established that the addition of copper can improve visible light absorption and efficiency of TiO2, however, little is known about the effect of these materials on supports i.e. monoliths for the photocatalytic reduction of CO2.

Many researchers have focused on ways of anchoring photocatalysts onto supports since high photoconversion efficiencies and improved light harvesting can only be achieved through the combined use of optimized photoreactor and photocatalyst configurations. Nishimura et al. dip coated TiO2 on a silica-alumina gas separation membrane to obtain 3.5ppmV/h of CO after 336 hours 9, while Pathak et al. used the hydrophilic structural cavities in Nafion-117 membrane films to host TiO2 coated with nanoscale silver and obtained methanol as the major product and formic acid as the minor product.10 Their results were reproducible even when these films were reused. Cybula et al. employed a flat perforated steel or plastic tray as a support for the dispersion of TiO2 in a tubular reactor designed for CO2 photoreduction studies.11 They observed that the type of support used not only played a critical role in determining the amount of immobilized catalyst, but also influenced the photoconversion rate when the same coating procedure was used. A decrease in catalyst loading and methane production (from 90ppm to 34ppm) was observed when the support was switched from steel to plastic due to weaker adhesive properties of plastic compared to steel.

The interconnected three-dimensional structures like the honeycomb monolith containing parallel straight channels has been exploited for industrial processes due to its potentially high surface to volume ratio, easy of scale-up through an increase of its dimensions and channels, control of structural parameters (i.e. pore volume, pore size and surface area) etc.12-13 Photocatalytic studies conducted using a monolith as support has identified low light utilization efficiency, due to little or no light absorption in the pores or channels of the honeycomb monolith.14 Not all immobilised photocatalyst may be activated due to limited light distribution arising from the catalyst coated on the outer surface absorbing most of the light 15. The light intensity also decays along the opaque channels of the monolith.16 More recently, it has been reported that the drawbacks of limited light penetration and efficiency of CO2 reduction can be improved by threading channels of monolithic structures with optical fibres.2, 17-18 Comparison of the slurry reactor system with the monolith system demonstrated that higher conversion and quantum

Catalysis Science & Technology Accepted Manuscript

efficiency can be achieved when the monolith was employed as a catalyst carrier.18 This was attributed to the combined advantages of the higher geometrical internal surface area of the monolith and the elimination of uneven light distribution via the optical fibres. Accordingly, experimental analyses using copper based nanomaterials immobilized onto monolithic structures threaded with optical fibres for CO2 reduction were conducted. Detailed characterization techniques were employed in order to investigate the effect of copper doping on the physicochemical properties of TiO2 based monoliths and correlate these properties to CO2 photoconversion.

2. Experimental

2.1 Preparation of copper based TiO2 monoliths

A series of Cu doped TiO2 monoliths within the range of 0.2 – 2 wt % were prepared by the sol-gel method (Fig.1). The monoliths were pre-coated with SiO2 sol prior to dip-coating in Cu-TiO2 sol. As shown in Fig.1, Cu-TiO2 sol was synthesized by adding a mixture of titanium (IV) butoxide and n-butanol to calculated amounts of copper (II) chloride dihydrate (CuCl2.2H2O) dissolved in 14ml of acetic acid. Subsequently, polyethylene glycol (PEG) solution was added to the metal loaded sol and stirred for 6 hours. The pre-coated SiO2 monoliths were then dip-coated in the resulting Cu-TiO2 sol for 30 minutes. The Cu-TiO2 coated monoliths and remaining sol were dried and calcined in a furnace at 150oC and 500oC, respectively. This procedure is detailed in previous work.18

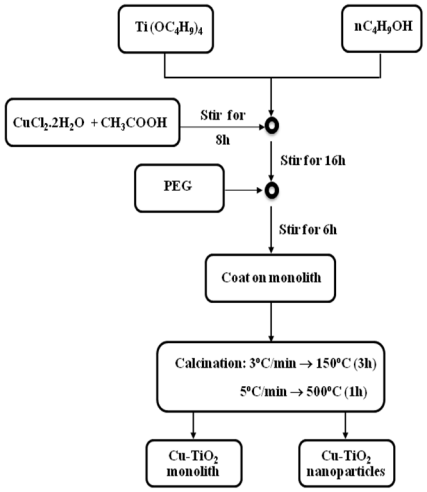

Fig.1 Sol-gel procedure for Cu-TiO2 monoliths

2.2 Photocatalyst characterization

Detailed information about the crystallographic structure of the sample showing the integrated intensity, peak positions, planes and unit cell parameters were obtained by using a Hiltonbrooks X-ray powder diffractometer with a Philips PW 1050 goniometer and proportional detector. The Nickel filtered Cu Kα radiation was used, operating at 20mA and 40kV with a scan range of 5-65 (2θ), scan speed of 2 degrees (2θ) per minute and step size of 0.05. The morphology of the nanoparticles were studied by transmission electron microscopy (TEM) using a JEOL 2100F instrument at an acceleration voltage at 200 kV. A Quanta 600 model equipped with energy dispersive X-ray (EDX) system was used to perform quantitative analysis and observe the morphology of the catalysts at the voltage of 25kV and 30kV, respectively. Specific surface area measurements were estimated from N2 adsorption-desorption isotherms at 77K that were measured using a ChemBET TPR/TPD analyzer connected to a linear mass flow controller/gas blender. The porosity and pore size distribution of the monoliths were characterized by a mercury (Hg) porosimetry analyzer (Micromeritics Autopore IV 9520 V1.05) with Hg pressure in the range of 0.7 – 275,790 kPa.

The elemental ratios of the metals contained within the nanoparticles were quantified by the Varian Vista MPX ICP-OES (inductively coupled plasma optical emission spectroscopy) system that used an echelle polychromator with a mega-pixel CCD detector. Prior to sample injection, approximately 25mg of Cu-TiO2 samples were digested in a mixture of 5ml of H2SO4 and 0.5ml of HClO4. The solution was then made up to 100ml in deionised water. X-ray photoelectron spectroscopy (XPS) was performed on the nanoparticles using a Kratos AXIS ULTRA instrument with mono-chromated Al kα X-ray source (1486.69 eV) operated at 15 mA emission current and 12 kV anode potential (180 W). High resolution scans were taken 5 or 10 minutes each over the appropriate regions for the photoelectron peaks with a step of 0.1 eV and pass energy of 20 eV. Wide/survey scans over the full energy range B.E. of 1400 –5 eV were performed on each sample at pass energy of 80 eV. The wide scans were used to estimate quantification of each element present based on the peak areas using CASAXPS software with Kratos sensitivity factors. The high resolution scans were charge corrected to the main C 1s peak = 285 eV and used to determine the chemical states of the elements detected. Spectral fitting was performed using CasaXPS software with a line shape based on a Gaussian/Lorentzian mix of 70:30 (GL30). The band gap, threshold wavelength and the absorbance of ultraviolet light as a function of the transmittance was measured by using the diffusive reflective ultraviolet-visible spectrophotometer (Varian Cary 300). The band gap energy of the samples were calculated using $Eg = hc/\lambda$ where h, c and λ represents the Planck's constant, velocity of light and wavelength, respectively.

2.3 Photoreduction of CO2

The photocatalytic reduction of CO2 under UVA or visible light was conducted in a cylindrical Pyrex glass reactor with volume of 216cm3. The catalyst coated ceramic honeycomb monoliths with 177 channels were threaded with optical fibres to ensure light distribution within the internal channels of the monolith. The humidifier was connected before the gas inlet, while the temperature and pressure were monitored via a type T thermocouple and pressure gauge, respectively, connected by 1/8" fittings after the product outlet. Light was irradiated into the side of the reactor by a light guide, with the illumination system being either a 200W mercury lamp or 500W halogen lamp, with light intensities of 33.42 and 68.35mW/cm2 respectively.

After performing a leak test with helium (He) gas, ultra pure CO2 (Air Products, 99.9995%) gas saturated with water vapour was bubbled into the reactor for 1 hour at flow rate of 4ml/min. Subsequently, the light source was turned on and readings were

Catalysis Science & Technology Accepted Manuscript

This journal is © The Royal Society of Chemistry [year]

taken after 4 hours. The flow of CO2 saturated with water vapour was continuous throughout the reaction. The H2O content in the feed was 50ml and pressure was maintained at 1 bar for every experimental run. Products extracted from extracted from the outlet of the gas-phase photoreactor were analyzed using a mass spectrometer (MS, Hiden Analytical) equipped with capillary, quadrupole mass analyser (HAL 201-RC) and Faraday/Secondary electron multiplier (SEM) detectors. Prior to every photocatalytic experiment, blank reactions were performed to confirm product formation was due to CO2 photoreduction.

3. Results and discussion

3.1 Textural properties of supported Cu catalysts

As shown in Fig. 2, the XRD diffraction patterns of TiO2 monoliths doped with different concentrations of copper consist mainly of two diffraction phases of anatase (A) and rutile (R). The rutile phase was detected in these samples at peak positions of 27.4o and 36.1o after calcination at 500oC. The crystallite size of all doped Cu-TiO2 based monoliths calculated from the Scherrer equation was within the range of 16.37 - 19.12 nm (Table 1). As the crystallite size of anatase decreased, an increase in rutile content was observed with increased metal concentration; with the 2wt%Cu-TiO2 sample showing maximum growth of rutile nuclei. This is due to the ability of Cu in enhancing the particle sintering process i.e. accelerating densification and grain growth, and thus promoting mineral phase transformation. 19

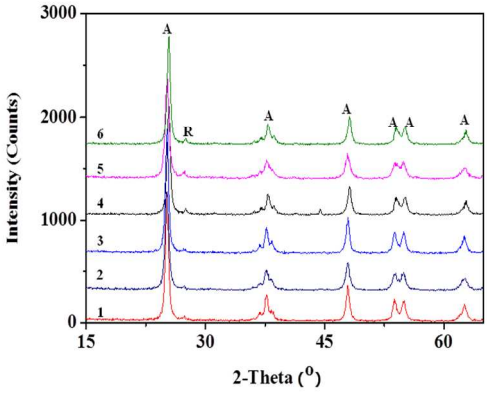

Fig. 2 XRD pattern of TiO2 monoliths with different Cu loading (1: TiO2, 2: 0.2wt%Cu-TiO2; 3: 0.5wt%Cu-TiO2, 4: 1wt%Cu-TiO2, 5: 1.5wt%Cu-TiO2, 6: 2wt%Cu-TiO2, anatase (A) and rutile (R))

These results suggest that the addition of Cu causes the gradual transformation of anatase to rutile with increasing metal concentration. The lattice constants (a & c) of Cu-TiO2 monoliths calculated based on the anatase (101) diffraction peaks, as listed in Table 1, increase with higher doping amount, when compared to the lattice parameters of TiO2 (a = 3.7892Å, c = 9.4803Å). Lattice parameter measurements were repeated thrice for verifying reproducibility. The standard error of the lattice parameter measurement via XRD is within the range of ± 0.05 - 0.28%. The lattice parameter of these Cu doped TiO2 monoliths increases as the crystallite size of anatase decreases.

The high resolution (HR) TEM images of 1wt%Cu-TiO2 using different magnifications illustrated in Fig. 3a shows aggregates of spherical nanocrystals with varying sizes from 5 - 27 nm. The SEM-EDS (energy dispersive spectroscopy) micrograph of the 1wt%Cu-TiO2 monolith presented in Fig. 3b confirms the presence of Cu, with the morphological features of the samples remaining unchanged by doping. The thickness of the 1wt%Cu-TiO2 film measured by SEM was up to 0.32µm on the surface of the monolith. The pore size distribution of the 1wt%Cu-TiO2 monolith measured by mercury porosimetry is illustrated in Fig. 4. The porosity and total intrusion volume for the 1wt%Cu-TiO2 sample was 35.04% and 0.17 mL/g while the pore size distribution was within the macropore range with the average pore diameter being 250Å.

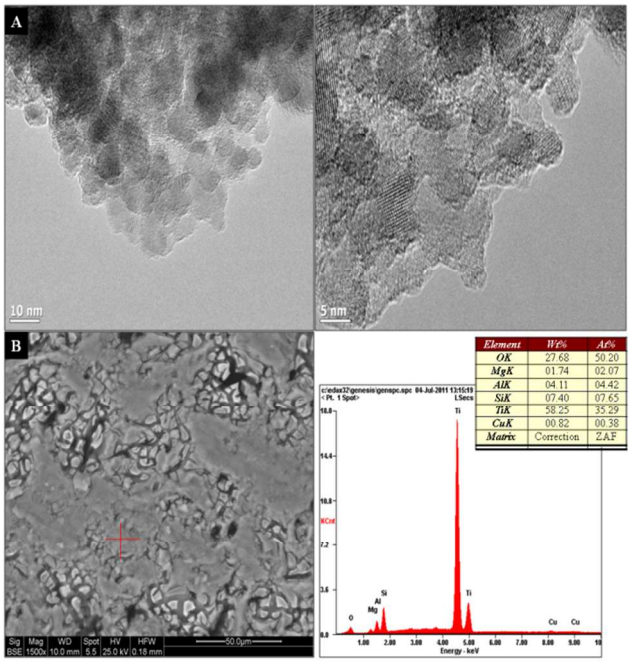

Fig. 3 TEM (A) and SEM-EDS (B) micrographs of 1wt% Cu-TiO2

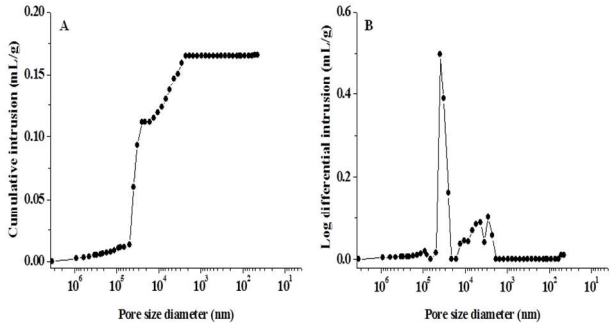

Fig.4 Pore size distribution measured by mercury porosimetry of the 1wt%Cu-TiO2 monolith showing the cumulative intrusion (A) and differential intrusion volume (B).

The BET specific surface area of the Cu-TiO2 based monoliths were within the range of 34.77 – 88.96m2/g (Table 1), and the standard error of these measurements is within the range of + 0.02 – 0.5%. An increase in specific surface area of TiO2 occurs

Catalysis Science & Technology Accepted Manuscript

with an increase in Cu loading.

Table 1 Physicochemical properties of the Cu-TiO2 based photocatalysts

Photocatalysts	Crystallite size (nm) / phase content (%)		Lattice parametersa		SBET (m2/g) b	ICP-OES	Band gap (eV)
	Anatase	Rutile	a (Å)	c (Å)		Cu (wt%)	
TiO2	12.99 (96.50)	4.91 (3.50)	3.7892	9.4803	52.50	0.00	3.08
0.2wt%Cu-TiO2	23.12 (96.70)	4.79 (3.30)	3.8039	9.4899	34.77	0.25	3.02
0.5wt% Cu-TiO2	19.12 (96.00)	5.97 (4.00)	3.8166	9.4943	37.52	0.53	2.96
1.0wt% Cu-TiO2	18.69 (94.60)	8.51 (5.40)	3.8186	9.4981	48.22	0.99	2.82
1.5wt% Cu-TiO2	18.29 (90.80)	8.77 (9.20)	3.8206	9.507	71.34	1.60	2.74
2.0wt% Cu-TiO2	16.37 (89.10)	25.51 (10.90)	3.8295	9.5242	88.96	2.03	2.61

a Estimated using Scherrer equation on (101) diffraction peak of anatase TiO2.

b BET surface area.

3.2 ICP-OES and XPS analysis

Table 1 lists the quantitative analysis calculated from ICP-OES. The ICP-OES analysis of Cu-TiO2 based monoliths demonstrated that Cu was present in the TiO2 matrix. The bulk elemental ratios of the samples are in agreement with the elemental concentration present in the precursor and show an increasing trend with increased metal concentration. This suggests that the added metals were primarily located in the crystal lattice via substitution of the Ti4+ ions with Cu2+ ions.

The high resolution XPS spectra of Cu 2p of Cu-TiO2 monoliths are presented in Fig.5. The Cu 2p3/2 and 2p1/2 peaks formed doublets with peak fitting suggesting that the chemical state is mainly Cu1+ with small amounts of Cu2+.20, 21 It has been reported that Cu may be reduced under the X-ray beam during XPS analysis.22 In the work presented here, three sets of scans were collected for each sample on three different areas. The experiment times were about 1 hour per area analysed with a monochromated source which has lower X-ray flux at the sample than a conventional 'flood' source. Nevertheless, it is possible that the Cu oxidation state started out before analysis proceeded, but analysis of auger peaks of Cu was not possible as scans were not recorded over sufficiently long exposure time to confirm reduction.

The intensity of the characteristic satellite peak for Cu2+ observed at 942.3 eV increased with increasing Cu concentration (Fig. 5).4 Colon et al. reported that the key difference between Cu1+ and Cu2+ species was the prominent satellite peak present on the high binding energy sides.23 These satellite peaks which have been reported to be responsible for the shakeup transitions by ligand to metal 3d charge transfer cannot be found in metallic Cu and Cu1+ species, due to their completely filled 3d shells.23 The satellite peaks were observed at 941.7 eV and 942.5 eV for 1wt% Cu/N-TiO2 and 1wt% Cu-TiO2 samples calcined at 600oC. Liu et al. also observed satellite peaks at 942.2eV and 942.4eV for 1wt% and 5wt% Cu-TiO2 samples prepared by simple precipitation, respectively.4 The XPS spectra of binding energies for Ti 2p were observed at 458.8eV and 464.6eV correspond to Ti4+ in TiO2.24-25 These results are in agreement with the literature, where Ti4+ peaks were observed at 457.7eV and 463.4eV for 1wt%Cu-10wt%I-TiO2 sample.24

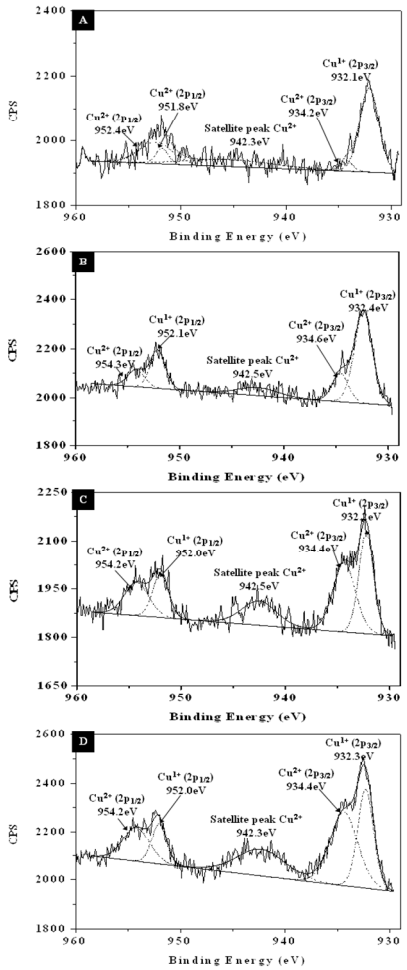

Fig. 5 XPS spectra of Cu 2p of Cu-TiO2 monoliths A) 0.5wt%Cu-TiO2, B) 1wt%Cu-TiO2 C) 1.5wt%Cu-TiO2 D) 2wt%Cu-TiO2

The XPS spectra of the O 1s region suggests that oxygen exists in

This journal is © The Royal Society of Chemistry [year]

Catalysis Science & Technology Accepted Manuscript

three forms on the sample surface with the binding energies of 529.5, 530.1 and 531.7eV. The main peak appears at 529.9eV and can be assigned to the bulk oxygen bound on TiO2. This value is consistent with the value of 530.1eV reported in the literature for anatase TiO2.21 The peak at 529.5eV probably corresponds to the O 1s peak of CuO 26 while the other peak at 531.7eV can be attributed to surface adsorbed components of hydroxyl (OH-) group.25, 27

3.3 Diffuse reflectance UV-Vis spectra of the Cu-TiO2 monoliths

The UV-Vis diffuse reflectance spectra of pure TiO2 and Cu-monoliths at various loading ratios are shown in Fig. 6. The absorption spectra of the resulting Cu-based TiO2 photocatalysts showed increased shift in the visible light with increased Cu loading concentration in comparison with pure TiO2. The band gap energies of these catalysts were within the range of 2.61-3.02eV. The lowest band gap energy was observed by the 2wt%Cu-TiO2 sample which is consistent with the literature, where increasing metal loadings results in a shift of the absorption edges of the TiO2 based samples.4-5, 7, 23 The defects created in the TiO2 network and crystalline structure is responsible for change in band gap energy 7. The absorption edge between 400-600nm can be attributed to the presence of surface defects created during annealing along with the crystallization of the rutile phase.28 Sahu and Biswas29 also observed increased absorption with increasing Cu2+ concentration. The change in light absorption was attributed to the incorporation of Cu1+ ions into TiO2 crystal lattice via the substitution of Ti4+ by Cu2+ atoms. Increased Cu2+ concentration was also reported to increase oxygen vacancies due to charge compensation effect.

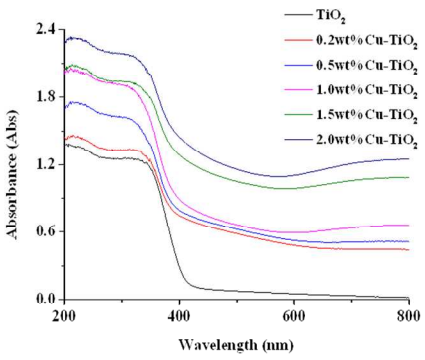

Fig.6 UV-Vis diffuse reflectance spectra of Cu-TiO2 monoliths

3.4 Photocatalytic reduction of CO2

The photocatalytic activities of the Cu-based TiO2 monoliths threaded with optical fibres were evaluated for CO2 photoreduction under UVA and visible light irradiation (Fig. 6). As shown in Fig. 7, several products such as hydrogen, methanol, acetaldehyde and ethanol were formed after 4 hours of light irradiation. The CO2 reduction experiments were repeated thrice, with the production rates averaged and the standard deviations reported in Fig. 7. The product rates steadily increases with an increase in metal concentration to give an optimal ratio of 0.5wt%Cu-TiO2 for the internally illuminated monolith photoreactor systems under either UVA or visible light irradiation, after which reduced product rates were observed for the subsequent higher doping ratios. Hydrogen and methanol were favourably produced; with maximum product rate of 12.55 µmol/gcath and 3.92 µmol/gcath, respectively under UVA (Fig. 7 (I)) and 3.73µmol/gcath and 0.23µmol/gcath, respectively under visible light irradiation (Fig. 7 (II)). The higher hydrocarbon evolution observed when the monolith was used as a catalyst carrier was due to the improved light distribution in the internally illuminated monolith photoreactor system.

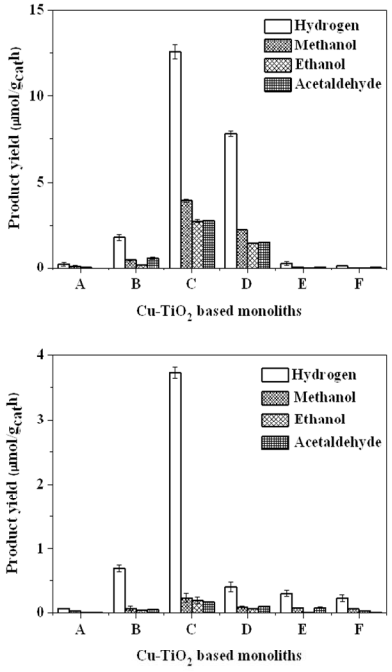

Fig.7 Effect of Cu doping on product rate using the monolith as a catalyst carrier under UVA (I) and visible (II) irradiation (A) TiO2, B) 0.2wt%Cu-TiO2, C) 0.5wt%Cu-TiO2, D) 1wt%Cu-TiO2 E) 1.5wt%Cu-TiO2 F) 2wt%Cu-TiO2

3.5 Correlation between catalyst characterization and yields of photoconversion

The improved photoreduction activity demonstrated by the 0.5wt%Cu-TiO2 coated monolith in UV and visible light region compared to pure TiO2 can be attributed to the incorporation of Cu1+ ions into the TiO2 matrix and good bi-crystallized TiO2 structure (i.e. crystallite phase of anatase with a small percentage of rutile). Phase transformation can be facilitated by substitutional dopants when cations enter the anatase lattice and cause an increase in the level of oxygen vacancies through valence or reduction / oxidation effects.30

Since the ionic radii of Cu1+ is similar to Ti4+, results from XRD confirm that the probability of substitutional doping occurring is high i.e. these metal ions occupying the lattice points of Ti. The decrease in crystalline size with increased Cu loading and lattice expansion observed in the diffraction patterns of the Cu doped samples explain the peak broadening observed which is associated with substitutional doping.

Nair et al. reported that cations with oxidation states of 3+ or lower tend to increase the oxygen vacancies in the lattice of TiO2 if placed within the lattice points.19 This increased concentration

Catalysis Science & Technology Accepted Manuscript

causes the subsequent rearrangement of atoms and reorganization of the structure for rutile phase in the lattice of TiO2 through the substitution of Ti4+ with cations.5, 30 Based on this, an increase in the concentration of oxygen vacancies will occur, which will enhance the nucleation process (i.e. anatase to rutile transformation) as also observed in this study.19

The phase transformation of Cu based TiO2 samples with increased metal concentration observed in this study were probably enhanced due to increased concentration of oxygen vacancies which simultaneously increased atomic mobility. Sahu and Biswas29 reported that the addition of metal dopants can alter the crystal phase of TiO2, with the degree of mineral phase transition being dependent on the metal type and concentration. This same phenomenon was observed by Nair et al.19, where increased enhancement was observed over CuO doped TiO2 samples compared to NiO doped TiO2. Colon et al.23 also observed lower anatase content with increased Cu concentration due to the higher amounts of dopants favouring the rutilization process. The influence of these substitutional ions is further confirmed by the change in light absorption properties and electronic structure of the metal loaded TiO2 samples observed in the UV-Vis spectra when compared to pure TiO2. According to Li et al.31, electronic states introduced by substitutional metal ions on the bottom of the conduction band edge of TiO2 cause the formation of a new higher unoccupied molecular orbital. This molecular orbital narrows the band gap; as also found in this study (Fig.6) and thus influences photon absorption.

The synergistic effect between the two crystalline phases in the Cu based samples could also be another plausible reason for improved activity. Improved charge separation and high reactivity at the anatase to rutile interface occurs during electron transfer from rutile to anatase at this interface where defect sites with unique charge trapping and adsorption properties can be created. 32-33 Bouras et al.33 and Zhang et al.34 reported that electron hole recombination can be retarded through the creation of energy wells and surface anatase/rutile phase junction which serve as electron traps formed from the lower band gap of rutile thus facilitating charge separation and increasing the lifetime of photogenerated electrons and holes. The presence of mixed crystalline phases of titania (i.e. anatase and rutile) has also been reported to show improved photocatalytic activity due to synergistic effect derived from better charge separation and high surface area. 35

After the optimal doping ratio of Cu1+ was exceeded within the series of synthesized catalysts (0.5wt %), reduced photoactivity was observed. This result could be due to the coverage of the surface of TiO2 with increased metal ions which inhibited interfacial charge transfer due to insufficient amount of light energy available for activation of all the catalyst particles. These results are in agreement with Li et al.36 where copper dopant below or above the optimum value of 0.5 wt% resulted in reduced production rates. The decrease in production rates at lower doping ratios below the optimum value was attributed to low Cu concentration while reduced catalytic activity at higher loadings were attributed to excess Cu species acting as recombination centres for photogenerated electrons and holes. When the doping content of Cu2+ exceeded 5 wt%, Tian et al.37 recorded a decrease in photocatalytic activity due to electron hole recombination. According to Schiavello38, photoreactivity can be negatively influenced by either a high concentration of metallic islands on the semiconductor surface or an enhancement of their size. When this occurs, reduced surface illumination of catalysts and increased recombination rate is observed.

4. Conclusions

The photocatalytic reduction of CO2 over Cu-TiO2 coated monolithic structures threaded with optical fibres was conducted under UV and visible light irradiation. The copper species present in the substitutional sites of the TiO2 matrix were found to modify the crystalline and optical properties of TiO2. Cu1+ was identified as the primary Cu species which facilitated multi electron reactions and thus improved the efficiency of CO2 photoreduction. The increase in Cu1+ concentration facilitated the anatase to rutile transformation due to the substitution of Cu1+ by Ti4+ in the TiO2 structure. Upon UV and visible light irradiation, the Cu doped photocatalysts exhibited improved activity compared to pure TiO2 at optimal doping ratios. The decline in production rate observed upon increased Cu1+ concentration was probably due to the coverage of the surface of TiO2 with excess metal particles. This inhibited interfacial charge transfer due to insufficient amount of light energy available for activation of the catalyst particles. More importantly, the improved conversion efficiency was probably due to improved charge separation at the anatase to rutile interface and the presence of Cu1+ species serving as electron traps which suppressed electron-hole recombination.

Acknowledgement:

We acknowledge the financial support from the School of Engineering and Physical Sciences and CICCS (EPRSC grant EP/F012098/2) at Heriot-Watt University. M. Maroto-Valer is grateful for the support from the Leverhulme Trust (Philip Leverhulme Prize). We thank Emily Smith, University of Nottingham, for XPS analysis.

Notes and references

a Centre for Innovation in Carbon Capture and Storage (CICCS), School of Engineering and Physical Sciences, Heriot-Watt University, Edinburgh, EH14 4AS, United Kingdom.
* Corresponding author at: School of Engineering and Physical Sciences, Heriot-Watt University, Edinburgh, United Kingdom. Fax: +44 (0)131 451 3180; Tel: +44 131 451 4737; E-mail: O.O.Ola@hw.ac.uk

1 D. Liu, Y. Fernandez, O. Ola, S. Mackintosh, M. Maroto-Valer, C. Parlett, A. Lee and J. Wu, Catal. Commun., 2012, 25, 78–82.
2 O. Ola and M. Maroto-Valer, J. Catal., 2014, 309, 300-308.
3 O. Carp, C. L. Huisman and A. Reller, Prog. Solid State Ch., 2004, 32, 33-177.
4 L. Liu, F. Gao, H. Zhao and Y. Li, Appl. Catal. B- Environ., 2013, 134-135, 349-358.
5 B. Xin, P. Wang, D. Ding, J. Liu, Z. Ren and H. Fu, Appl. Surf. Sci., 254, 2569-2574.
6 J. Li, J. Zeng, L. Jia and W. Fang, Int. J. Hydrogen Energ., 2010, 35, 12733-12740.
7 H. Slamet, E. Purnama, K. Riyan and J. Gunlazuardi, Catal. Commun. 2005, 6, 313-319.

Catalysis Science & Technology Accepted Manuscript

This journal is © The Royal Society of Chemistry [year]

8 H. Slamet, E. Purnama, K. Riyan and J. Gunlazuardi, World Appl. Sci. J., 2009, 6, 112-122.
9 A. Nishimura, N. Komatsu, G. Mitsui, M. Hirota and E. Hu, Catal. Today, 2009, 148, 341-349.
10 P. Pathak, M. Meziani, L. Castillo and Y. Sun, Green Chem., 2005, 7, 667-670.
11 A. Cybula, M. Klein, A. Zielińska-Jurek, M. Janczarek and A. Zaleska, Physicochem. Probl. Mi., 2012, 48, 159-167.
12 K. Nakata and A. Fujishima, J. Photoch. Photobio. C, 2012, 13, 169-189.
13 H. Lin and K. Valsaraj, J. Appl. Electrochem., 2005, 35, 699-708.
14 Y. Yu, Y. Pan, Y. Wu, J. Lasek and J. Wu, Catal. Today, 2011, 174, 141-147.
15 M. Dijkstra, H. Buwalda, A. W. F. de Jong, A. Michorius, J. G. M. Winkelman and A. A. C. Beenackers, Chem. Eng. Sci., 2001, 56, 547-555.
16 M. Singh, I. Salvadó-Estivill and G. Puma, AICHE J., 2007, 53, 678-686.
17 P. Liou, S. Chen, J.C. Wu, D. Liu, S. Mackintosh, M. Maroto-Valer and R. Linforth, Energy. Environ. Sci., 2011, 4, 1487–1494.
18 O. Ola, M. Maroto-Valer, D. Liu, S. Mackintosh, C. Lee and J. Wu, Appl. Catal. B-Environ., 2012, 126, 172-179.
19 J. Nair, P. Nair, F. Mizukami, Y. Oosawa and T. Okubo, Mater. Res. Bull., 1999, 34, 1275-1290.
20 C. D. Wagner, A. V. Naumkin, A. Kraut-Vass, J. W. Allison, C. J. Powell and J. R. Rumble, NIST X-ray Photoelectron Spectroscopy Database, 2007, 20 Version 3.5.
21 M. Biesinger, L. Lau, A. Gerson, and R. Smart, Appl. Surf. Sci., 2010, 257, 887-898.
22 C. Chusuei, M. Brookshier and D. Goodman, Langmuir, 1999, 15, 2806-2808.
23 G. Colon, M. Maicu, M. Hidalgo and J. Navio, Appl. Catal. B-Environ., 2006, 67, 41-51.
24 Q. Zhang, T. Gao, J. Andino and Y. Li, Appl. Catal. B-Environ., 2012, 13, 257-264.
25 Q. Zhang, Y. Li, E. Ackerman, M. Gajdardziska-Josifovska and H. Li, Appl. Catal. A-Gen., 2011, 400, 195-202.
26 E. Z. Kurmaev, V. R. Galakhov, V. V. Fedorenko, L. V. Elokhina, S. Bartkowski, M. Neumann, C. Greaves, P. Edwards, M. Al-Mamouri and D. L. Novikov, Phys. Rev. B, 1995, 52, 2390-94.
27 Y. Wang, B. Li, C. Zhang, L. Cui, S. Kang, X. Li and L. Zhou, Appl. Catal. B-Environ., 2013, 130-131, 277-284.
28 A. Heciak, A. Morawski, B. Grzmil and S. Mozia, Appl. Catal. B-Environ., 2013, 140-141, 108-114.
29 M. Sahu and P. Biswas, Nanosc. Res. Lett., 2011, 6, 441-454.
30 D. Hanaor and C. Sorrell, J. Mater. Sci., 2011, 46, 855-874.
31 W. Li, A. Frenkel, J. Woicik, C. Ni and S. Shah, Phys. Rev. B, 2005, 72, 155315-155321.
32 J. Carneiro, T. Savenije, J. Moulijn and G. Mul, J. Phys. Chem. C, 2011, 115, 2211-2217.
33 P. Bouras, E. Stathatos and P. Lianos, Appl. Catal. B-Environ., 2007, 73, 51-59.
34 J. Zhang, Q. Xu, Z. Feng, M. Li and C. Li, Angew. Chem. Int. Edit., 2008, 47, 1766-1769.
35 K. Schulte, P. DeSario and K. Gray, Appl. Catal. B-Environ., 2010, 97, 354-360.
36 Y. Li, W. Wang, Z. Zhan, M. Woo, C. Wu and P. Biswas, Appl. Catal. B-Environ., 2010b, 100, 386-392.
37 C. Tian, Y. Zhao, J. Zhang and C. Zheng, in Cleaner Combustion and Sustainable World, Springer-Verlag, Berlin, 2013.
38 M. Schiavello, Heterogeneous Photocatalysis, John Wiley and Sons, Chicester, 1997.

Catalysis Science & Technology Accepted Manuscript